Deposition of Hydroxyl Functionalized Films by Means of ethylene Aerosol-Assisted Atmospheric Pressure Plasma

Yi-Wei Yang,† Giuseppe Camporeale,† Eloisa Sardella, Giorgio Dilecce, Jong-Shinn Wu, Fabio Palumbo,* Pietro Favia*

The atmospheric pressure plasma deposition of hydroxyl functionalized hydrocarbon films is reported in this work, with a reactor fed with water aerosol and ethylene. The effects of power and feed flow rates onto film chemistry have been investigated. Coatings produced with this approach can find application in the biomedical field, among others, as platforms for cell adhesion and proliferation. Results show that operating at 4 kHz provides a much higher amount of hydroxyl group in the coating compared with samples obtained at 11 kHz. After water immersion, the stability of the films and their amount of hydroxyl groups remain high. A simplified deposition mechanism is proposed.

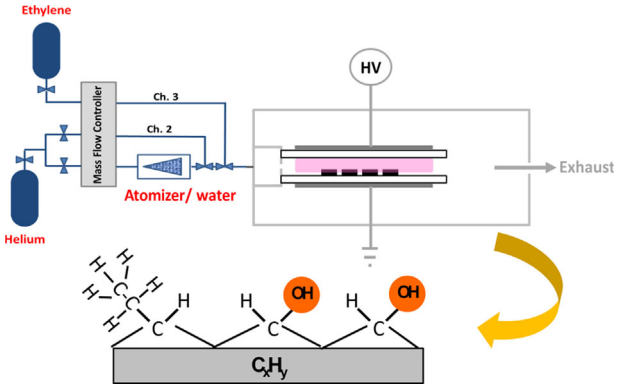

1. Introduction

In the last two decades, coatings functionalized with carbonyl, carboxylic, hydroxyl, amine, and ethylene oxide (—CH_2CH_2O—) ether groups have been extensively studied and proved to be appropriate for biomedical applications such as: protein, DNA, and biomolecules immobilization; cell adhesion and growth; biosensor fabrication; and non-fouling surfaces.[1–21]

Hydroxyl functional groups are interesting for cell adhesive surfaces and biomolecule immobilization, for their polar weakly acid character, and reactivity. —OH groups could be easily accessed for grafting bioactive molecules by mild reactions,[22,23] in order to provide functionalized surfaces for bio-devices and bio-sensors development, just aiming to the biomedical field.

Wet chemical synthesis is one of the approaches for functionalized polymers, in which two strategies, direct functional polymerization and post-functionalization, are commonly employed. However, they usually suffer from time consuming tedious operations and poor yield, which barely fits industrial requirements.[22,24–27]

Plasma deposition processes allow rapid, simple, one-step protocols, for providing coatings with pre-determined variable structure (crosslinking, roughness, and porosity)

Dr. Y.-W. Yang, Dr. J.-S. Wu
Department of Mechanical Engineering, National Chiao Tung University, Hsinchu, Taiwan
Dr. G. Camporeale, Dr. P. Favia
Dipartimento di Chimica, Università degli Studi Aldo Moro, Bari, Italy
E-mail: pietro.favia@uniba.it
Dr. E. Sardella, Dr. G. Dilecce, Dr. F. Palumbo, Dr. P. Favia
Consiglio Nazionale delle Ricerche, Istituto di Metodologie Inorganiche e dei Plasmi, Bari, Italy
E-mail: fabio.palumbo@cnr.it

†These authors contributed equally to this work.

DOI: 10.1002/ppap.201400066

chemical composition and stability in water and other media, well adherent to substrates.[28,29]

Considerable efforts have been devoted to the investigation of low pressure plasma deposition processes of coatings functionalized with carboxylic, hydroxyl, and amine groups using different monomers, e.g., acrylic acid, allyl-alcohol, and allyl-amine, respectively.[30–39]

Typically, these processes were optimized in vacuum conditions, that offer very high process versatility and established scientific background; disadvantages are encountered due to: the complexity and the cost of the pumping systems; the low deposition rate when mild conditions are used for improving the retention of the monomer structure in the coatings; the low flow rate for high-boiling monomers; and outgassing substrate materials.

Since years atmospheric pressure plasma (APP) deposition processes attracts academic and industrial researchers due to: possible advantages such as lower cost with respect to expensive vacuum pumps; easy operation, and implementation in industrial lines.[8,40–42] In most cases, confinement of the plasma processing electrode area has to be considered, though, for safety and for limiting contamination of the feed. Further, in APP deposition processes the ion bombardment of the substrate is negligible, also for this reason the adhesion of the coatings to the substrates need more careful optimization with respect to low pressure conditions. Dielectric barrier discharge (DBD) is the most popular configuration for APP deposition processes, allowing easy implementation, large working area, and potential for scale up.[43,44]

As at low pressure, in APP processes acrylic acid is among most investigated monomer for introducing carboxylic groups on substrate surfaces to elicit cell attachment and proliferation.[45–48]

Studies on biomedical applications report also on APP deposition processes from methyl methacrylate for surfaces functionalized with ester groups, suitable for prosthesis and implants.[49] Recently, the authors of this paper published a research on APP deposition processes of polylactic acid-like[50] and PEO-like[18] coatings.

Deposition processes of hydroxyl functionalized coatings from alcohol precursors have been thoroughly investigated in low pressure plasma[51–57]; on the contrary few papers report on work aimed at depositing such films in APP conditions from OH-bearing monomers (such as hydroxyethylmethacrylate or propargyl alcohol).[58,59] To the best of our knowledge, literature does not account for the modulation of hydroxyl content in APP polymerized coatings from a water/hydrocarbon feed. Furthermore, it should be highlighted that decoupling the flow rate of the OH radicals precursor (H_2O) from the one of the film building block source (an hydrocarbon monomer) can allow a finer tuning of the chemistry, with respect to a plasma system fed with an alcohol (or alike). In fact in the former case the flow rate ratio is an additional parameter for managing the grafting of OH groups in the coating.

In recent years, aerosol-assisted APP deposition processes emerged as novel approach to the plasma deposition of functionalized coatings.[18,60–64] This technique allows the direct injection in APP systems of "mist" (aerosol) of pure liquid monomers, solutions, and nanoparticle suspensions. Within this approach, the atomization of the liquid provides higher amount of low vapor pressure monomers in the feed compared with common bubblers, with a limited temperature dependence.[65] This approach allow to feed plasma with high boiling monomers, without need for heating, and with solutions of complex, non-volatile species such as most biomolecules, with consequent increase of the structure retention of the monomer in the coating, and high deposition rate compared with low pressure systems.[50,66,67]

In the present study, OH-functionalized hydrocarbon films have been deposited in a DBD equipment fed with a water/ethylene/helium mixture, whereas H_2O is injected in aerosol form through an atomizer. Ethylene has been chosen for the well-known good polymerization rates and reaction mechanism in DBDs.[68,69] Chemical composition and morphology of the deposited coatings have been investigated, and a simplified deposition mechanism is proposed.

2. Experimental Methods

2.1. Reactor Set-Up and Experimental Deposition Conditions

The APP reactor is schematically represented in Figure 1. It consists of two parallel plate silver electrodes, $8 \times 13\ cm^2$ wide, 5 mm apart, both covered with 0.6 mm thick alumina sheets. The gas feed is let between the electrodes from one side, the opposite side was connected to an aspirator hood. Helium (99.999%, Air Liquide) at 5 slm and ethylene (99.95%, Air Liquide) at 10 sccm, carrier gas and deposition precursor, respectively, were fed through electronic mass flow controllers (MKS Instruments). ethylene aerosol was added to the feed with an atomizer (mod. 3076, TSI) operated with He in the 2–5 slm flow rate range. The total He flow rate (carrier and atomizer) was kept constant at 5 slm in all deposition conditions reported in this paper.

Since un-atomized water was re-circulated and returned in the water reservoir of the atomizer, the mass flow rate of the water aerosol was properly calibrated from the weight difference of the reservoir in each deposition condition.

A quite linear increase of the water mass flow rate, in the range 6–111 mg min^{-1} resulted by increasing the atomizer

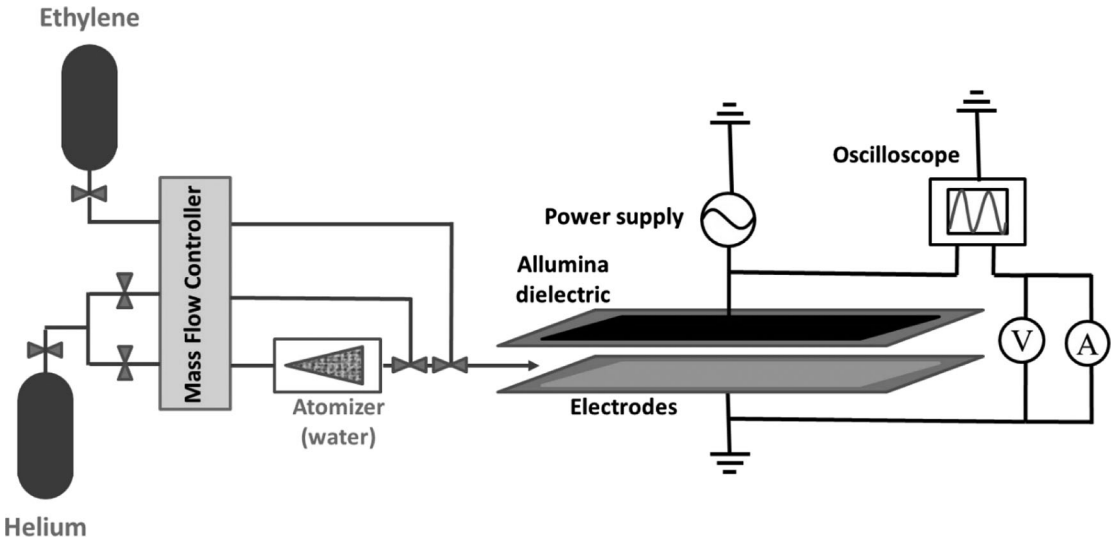

Figure 1. Schematic diagram of aerosol-assisted atmospheric pressure dielectric barrier discharge deposition system.

flow rate from 2 to 5 slm. For sake of clarity, being a more operative parameter, in the text the results are reported as a function of the atomizer flow rate.

The discharges were ignited using an AC power supply consisting of a function generator (TG1010A, ThurlbyThandar instruments), an amplifier (Industrial Test Equipment Powertron 1000A) and a high-voltage transformer (Amp Line). The applied voltage was kept at 6 kV_{pp} at 4 and 11 kHz. Before running the process, the system was purged with 5 slm He for 5 min. Each discharge was run for 10 min on $2.4 \times 2.4\ cm^2$, 710 μm thick, shards of double side polished p-Silicon wafer (MicroChemicals GmbH, Ulm, Germany), placed in the center of the electrode. Detailed operation conditions are listed in Table 1

The electrical properties of the plasma were investigated for determining the voltage and the current delivered to the system; a high-voltage (P6015A, Tektronix) and a resistance type current probe were utilized, both connected to an oscilloscope (TDS 20145C, Tektronix). The power delivered was obtained multiplying the energy per voltage cycle by the frequency. The energy per cycle was calculated from the time integral of the current times the voltage in one cycle, which is equivalent to the area of the charge (Q) versus V Lissajous figure.[70] This calculation provides an average power value. Passing from 4 to 11 KHz, the energy/cycle does not change appreciably, so that the (average) power rises due to the frequency increase. Since at higher frequency the energy per cycle is delivered in a reduced time, the equal energy/cycle value is due to a larger current in a shorter time in each discharge event (two in one voltage cycle). From now on, we shall call power density the average discharge divided by the electrodes surface ($W\ cm^{-2}$), a parameter that is commonly found in literature.

Table 1. Water–ethylene plasma deposition parameters.

Experimental parameters			
Frequency	4 kHz		11 kHz
Applied voltage		6 kV_{pp}	
Power density	0.3–0.4 $W\ cm^{-2}$		0.9–1.3 $W\ cm^{-2}$
Voltage waveform		Continuous wave – sinusoidal	
Ethylene flow rate		10 sccm	
Total He flow rate		5 slm	
He flow rate through atomizer		0–5 slm	

DOI: 10.1002/ppap.201400066

2.2. Coating Characterization

The thickness of the coatings was measured with a profilometer (KLA D-120 Tencor) and presented as average values of at least three measurements in the same condition. The morphology inspection of film top and cross-sections was carried out with a scanning electron microscope (SEM Zeiss Supra 40, equipped with a field emission Gemini column) under an extraction voltage of 3 kV after sputter metallization with 15 nm Cr.

Water contact angle (WCA) measurements were performed in static (θ_s), advancing (θ_a), and receding (θ_r) mode with a CAM 2008 (KSV Instruments), goniometer equipped with a CCD camera. Water drops of 2–4 μl were used.

X-ray photoelectron spectroscopy (XPS) surface characterization of the coatings were performed with a Thermo Fisher Scientific Theta Probe Spectrometer, by using monochromatic X-rays (300 μm diameter spot). Survey and High-Res spectra were acquired at a pass energy of 150 and 100 eV, respectively, in constant analyzer energy (CAE) mode. Charging effects were compensated with a flood-gun. Calibration of the binding energy (BE) scale was performed by setting the aliphatic C1s component at 285.0 eV. Curve-fitting analysis (Smart type background; and Gaussian/Lorentzian peaks), was applied to all High-Res spectra; the Thermo Avantage software (v. 5.24, Thermo Fisher Scientific) was used.

Fourier transform infrared spectroscopy (FT-IR) was carried out to characterize the bulk of the coatings. FT-IR spectra (32 scans, 4 cm^{-1} resolution) were obtained in transmission mode with a Vertex 70V Bruker spectrometer. The spectrometer was evacuated to less than 150 Pa for 5 min before spectrum acquisition to avoid interferences due to atmosphere and the spectra were normalized by the thickness. OH/CH and C=O/CH signal ratios were calculated from the peak areas of O—H (3 650 cm^{-1}), CH (2 780–3 000 cm^{-1}), and C=O (1 640–1 840 cm^{-1}) bands. Background subtraction, integration of peak areas, and other operations were performed with Opus 5.0 software.

3. Results and Discussion

3.1. FTIR Analysis

FTIR analysis allowed the identification of chemical bonds and functional groups in the coatings. Figure 2 reports the normalized FTIR spectra of films deposited under various atomizer flow rate and frequency conditions. The intensity of OH (broad band at 3 636–3 150 cm^{-1}), C=O (1 708 cm^{-1}), and C—O (1 056 cm^{-1}) stretching bands become more intense with water aerosol injection both at 4 and 11 kHz. In particular, it should be stressed that the hydroxyl contribution is negligible, and other oxygen containing groups as well, without H_2O addition. A successful functionalization of the H_2O aerosol-assisted deposited coatings is thus confirmed. It is worth to note that the spectra of these coatings exhibit great similarity with those plasma-deposited from allyl-alcohol in low pressure conditions.[56]

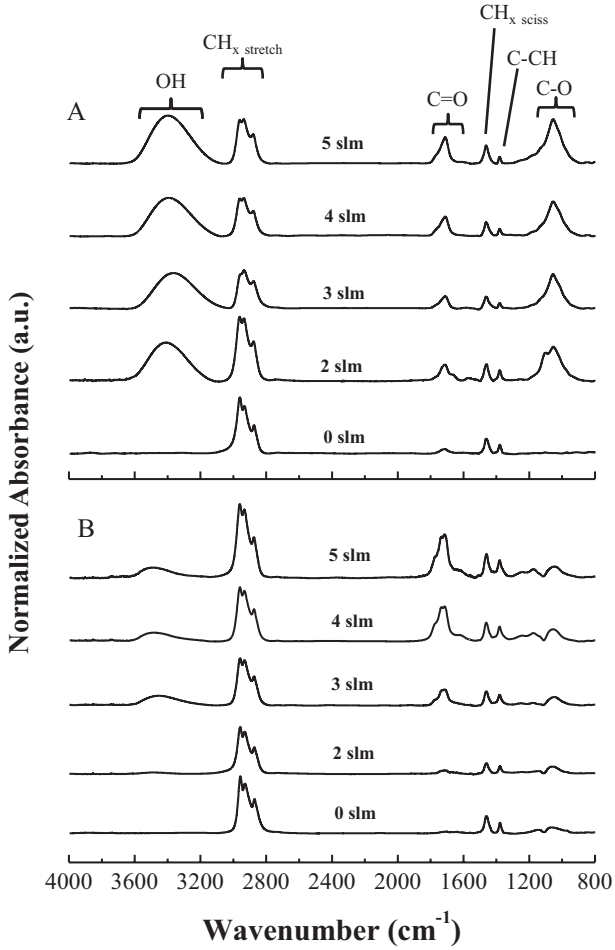

Figure 2. FTIR analysis of films deposited at different atomizer flow rates and frequency, 4 kHz (a) and 11 kHz (b).

Table 2 shows the OH/CH and C=O/CH band intensity ratios as a function of the experimental parameters for

Table 2. Relative FTIR area intensity ratio of OH and C=O with respect to CH in function of atomizer flow rate and frequency.

Atomizer flow [slm]	4 kHz		11 kHz	
	OH/CH	C=O/CH	OH/CH	C=O/CH
0	0	0.1	0	0
2	1.4	0.2	0.1	0.1
3	2.4	0.2	0.4	0.3
4	2.5	0.3	0.3	0.6
5	2.8	0.4	0.2	0.6

presenting the relative concentration trends of the functional groups within the coatings. The results at 4 kHz reveal an increasing trend for OH and C═O groups with raising the aerosol flow rate. At 11 kHz, instead, the OH/CH and C═O/CH ratios increase till 3 slm of He atomizer flow rate is used, then remain fairly constant or decrease (in the case of OH groups). It should be highlighted that, at 4 KHz, a OH/CH ratio as high as 2.8 can be found with the highest aerosol flow rate (5 slm). Furthermore, at 4 kHz, aerosol flow rates over 2 slm leads to quite high OH/C═O ratios, in the range 7–12, while at 11 kHz such ratio does not change too much, or it is in favor of the carbonyl group. This outcome clearly indicates that a certain selectivity toward OH groups can be obtained in this deposition process by properly tuning the frequency of the field applied to the DBD, and in turn the power density. It should be considered that, the broad C═O band in the spectra represents both carbonyl groups and more oxidized carbon (such as in esters, anhydrides, or carboxylic acids). On the other hand, besides R—OH groups, acid ones can contribute to the band at 3 400 cm^{-1}. Hence comparison with XPS data is important to better discriminate the functional groups.

3.2. XPS Analysis

Comparing FT-IR with XPS data allows to better understand the distribution of functional groups in the coatings. Surface composition XPS data are reported in Table 3, where the addition of oxygen functionalities in the coatings is confirmed both at low and high frequencies. It can be observed that at 4 kHz the O/C XPS ratio follows the increasing trend of the oxygen containing groups obtained by FTIR analysis (Table 2). A lower trend of the O/C ratio is found in coatings deposited at 11 kHz, with a maximum at around 4 slm of atomizer flow rate. Both trends are in agreement with FT-IR data. Indeed, also coatings deposited from ethylene, with no water addition, evidence the presence of oxygen. This can be likely ascribed to well-known inevitable post-oxidation of the coatings at the atmosphere, or reaction with water vapor or oxygen desorbed from the electrodes during the process.[71]

Table 3. Atomic ratio and concentration of C1s and O1s for plasma-deposited water–ethylene films.

Atomizer flow rate [slm]	4 kHz			11 kHz		
	C1s [%]	O1s [%]	O/C	C1s [%]	O1s [%]	O/C
0	91.1	8.9	0.10	94.7	5.3	0.06
2	90.4	9.6	0.11	93.8	6.2	0.07
3	78.3	21.7	0.28	87.3	12.7	0.14
4	77.8	22.2	0.29	86.1	13.9	0.16
5	75.6	24.4	0.32	90.4	9.6	0.11

Figure 3a–d shows the best-fitted C1s signal for the coatings deposited without (0 slm) and with the highest water aerosol flow (5 slm),at low and high frequency. It can be observed that at 4 kHz the abundance of C—O moieties is much more relevant than the other oxidized components when water aerosol is added (trace b). At 11 KHz, hence at higher power density, the reduced efficiency of the plasma in selectively grafting hydroxyl groups is confirmed: in fact, at 5 slm of water aerosol flow rate (trace d) the C—OH/C—O—C component has an abundance close to the C═O/O—C—O one. Both XPS and FT-IR data confirm that at lower power density more —OH groups are included in the coatings.

3.3. WCA Measurements

The wettability of the functionalized coatings was evaluated through advancing, receding and static WCA measurements; WCA data are reported in Figure 4. The increase in wettability, due to incorporation of oxygen containing groups, is demonstrated for coatings deposited at 4 kHz since the static and receding contact angle decreases when a water atomizer flow rate higher than 2 slm is used. When the atomizer flow exceeds 3 slm, the static and receding angles reach a minimum value around 50° and 18°, respectively. Furthermore, a high hysteresis can be observed, which cannot be ascribed to the roughness of the coatings; since SEM observations, shown in Figure 5, indeed indicate a quite flat surface in all deposition conditions. Thus the WCA hysteresis should be due to the chemical composition of the coating, and its interaction with water.

Little WCA changes are observed, instead, in coatings deposited at 11 kHz, when more water is added to the feed. This is in agreement with FT-IR and XPS data shown previously, and with the fact that a low density of O-containing polar groups is included in the coatings deposited at higher power frequency.

3.4. Deposition Rate

The deposition rate for coatings deposited both at 4 and at 11 kHz are reported in Figure 6 as a function of the water addition (atomizer flow rate) and of the field frequency. At 4 kHz, the deposition rate exhibits a raising trend with the water aerosol addition, reaching values as high as about 68 nm min^{-1}, only slightly influenced by He flow rate higher than 3 slm. In contrast, at 11 kHz a decreasing trend for the growth rate is found with increasing the atomizer flow rate, from 95 to about 30 nm min^{-1}. It is important to consider that without water aerosol, i.e., in conditions

DOI: 10.1002/ppap.201400066

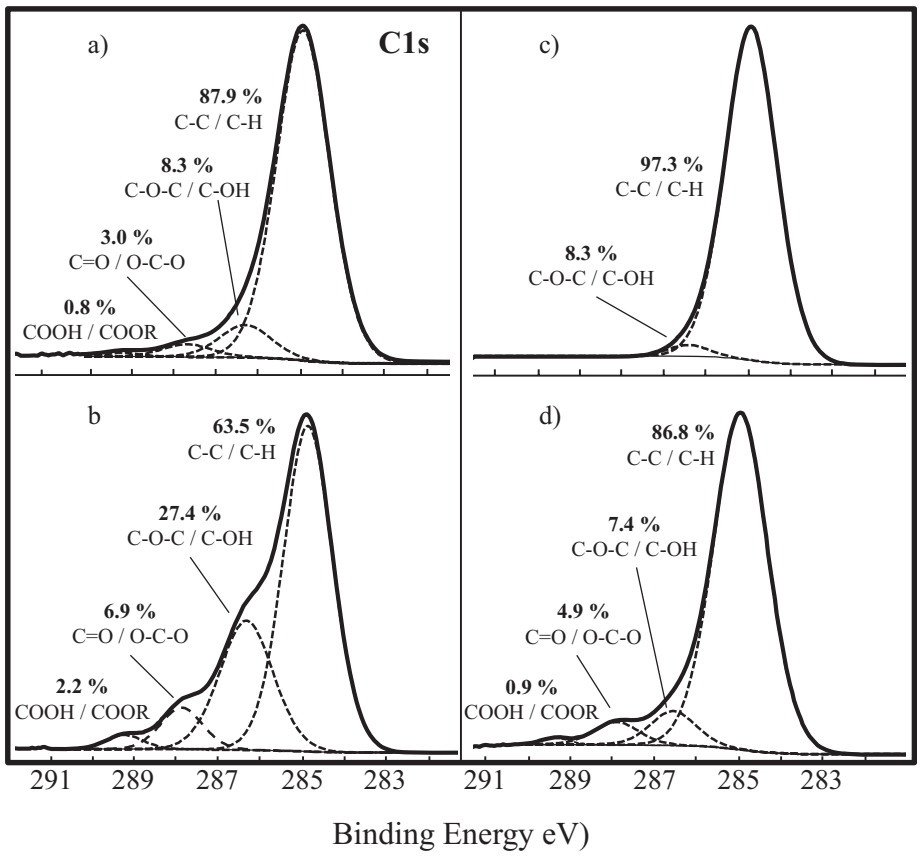

Figure 3. Best fitting of C1s spectra: 4 kHz (a, b) and 11 kHz (c, d) at atomizer flow rate of 0 (a, c) and 5 slm (b, d).

leading to hydrocarbon films, the deposition rate at 11 KHz is much higher.

These outcomes highlighted the different effect of water addition in the feed at different power density, pointing out to relevant changes in feed fragmentation and composition of the plasma. In particular, a competition of depositing (hydrocarbon species) and etchant (oxygen and H atoms) species can be hypothesized, whose relative contribution depends on the power applied.

According to the results and the latter speculation, a simplified surface reaction mechanism can be proposed as schematized in Figure 7. It can be supposed that the

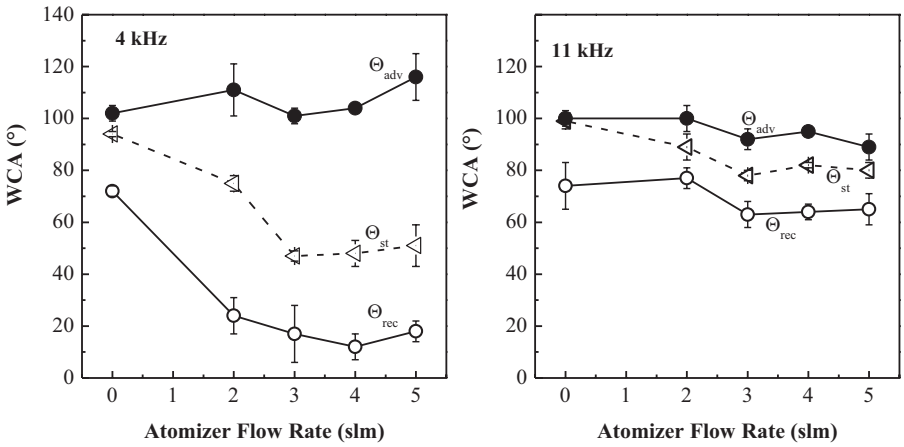

Figure 4. Advancing, static, and receding water contact angle measurements of films deposited at 4 and 11 kHz and at different atomizer flow rates.

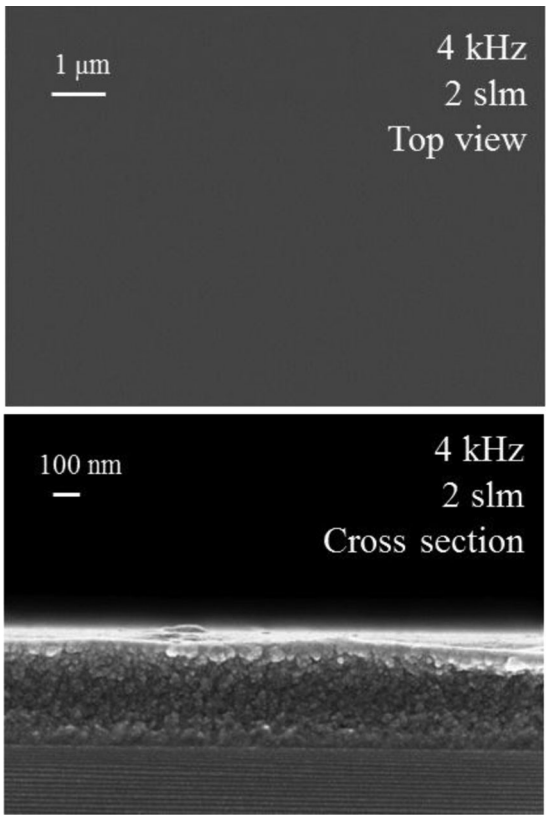

Figure 5. SEM top and cross-section view of a water–ethylene plasma deposited film (4 kHz, 2 slm of atomizer flow rate).

monomer mostly contributes to the formation of polymer precursors, CH_x radicals and alike, while water mainly produces OH radicals, hydrogen (also originated from ethylene), and oxygen atoms by dissociation or dissociative recombination reactions.[72,73]

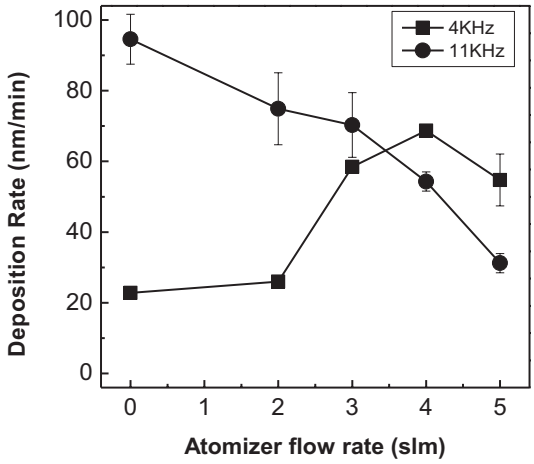

Figure 6. Deposition rates of films deposited at 4 kHz (squares) and 11 kHz (circles) at different atomizer flow rate.

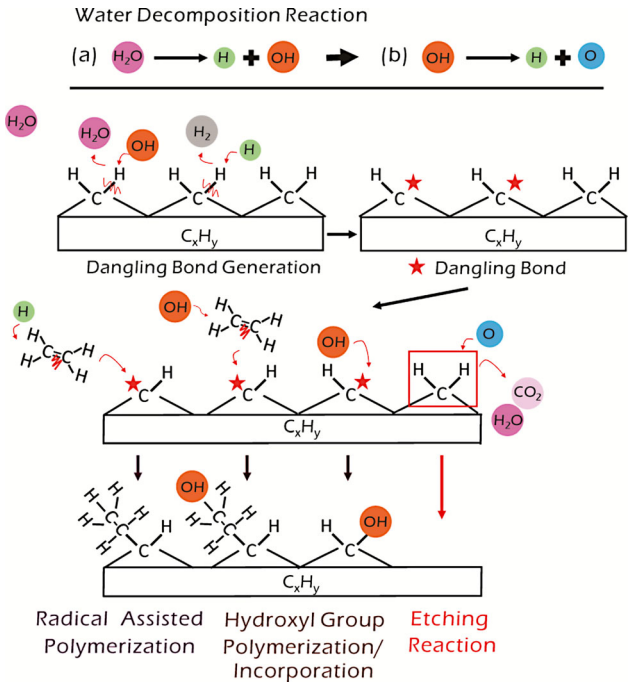

Figure 7. Hypothesized water decomposition and surface reaction mechanism.

The latter species certainly can be responsible for etching of the growing film, whereas as well demonstrated in the past, OH radicals have a high reactivity with hydrocarbon polymers leading to surface grafting. On the other hand, both hydroxyl radicals and H atoms are known to trigger surface bonded hydrogen abstraction hence promoting both polymer growth, through formation of active sites, and enhanced reactivity of the surface toward etching reactions.[74–76]

The chemical analysis and deposition rate results can be rationalized considering that water is mostly involved into two main broad reactions (indicated as (a) and (b) in Figure 7): water dissociation in H and OH radicals, and then the latter giving rise to O atoms. It is reasonable to suppose that at low frequency, hence at lower power, channel (b) is less relevant, and hydrogen atoms and hydroxyl radicals can actively react with C—H bond on polymer surface enhancing the formation of dangling bonds as well as reacting with ethylene, thus contributing to monomer activation. Both processes lead to enhanced film growth rate. On the other hand, the dangling bonds can also react with OH radicals promoting hydroxyl groups incorporation. In the low power density scenario, water addition can lead to deposition rate (at constant monomer feed flow rate) and hydroxyl groups addition increase. In the conditions leading to higher power density, i.e., at higher frequency, an increased production of film precursors is expected by monomer fragmentation, thus the deposition rate at low

DOI: 10.1002/ppap.201400066

water addition is quite higher than the one obtained at low frequency. However, it can be supposed that channel (b), leading to formation of the etchant species (O atom), becomes more relevant when the power is increased, thus at higher water addition (atomizer flow rate) the deposition rate fairly decreases, as a result of film etching.

3.5. Stability in Water

In order to evaluate the stability in water of the deposited films, the changes in terms of film thickness and FITR absorption spectra before and after water immersion were investigated. Figure 8 shows film thickness variation after immersion in distilled water for 1 and 7 d of coatings deposited from C_2H_4/H_2O/He (with 5 slm He of atomizer flow rate) and C_2H_4/He feeds. It can be seen that coatings deposited in water-free conditions, along with those deposited at 11 kHz with 5 slm of H_2O/He aerosol reveal nearly no difference in thickness after water immersion, thus they can be considered stable in water.

The coating deposited at lower frequency and with the highest atomizer flow rate (5 slm), instead, shows a thickness decrease from about 650 to 500 nm after 1 d of immersion. Afterward, considering the 7 d immersion, it can be observed that the coating undergoes almost no further changes, denoting that after releasing in water some loosely bonded polymer portions in the first 24 h, the remaining film is quite stable.

Figure 9 shows the corresponding FTIR spectra of films tested for the water soaking stability: the results indicate consistency with what observed in terms of thickness

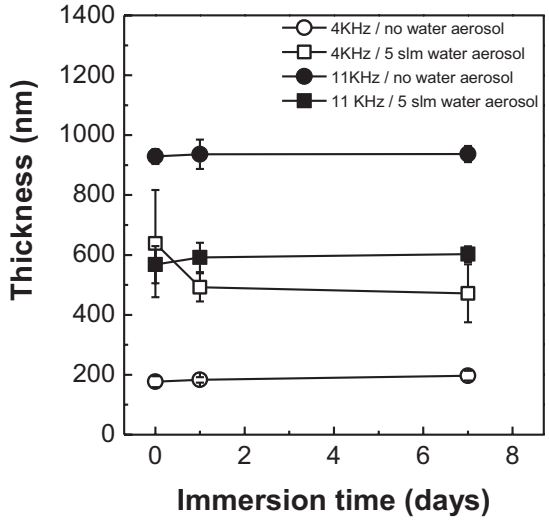

Figure 8. Thickness variation of deposited films in time upon water immersion. Circles: no water atomization; squares: 5 slm He aerosol. White and full symbols: coatings deposited at 4 and 11 KHz, respectively.

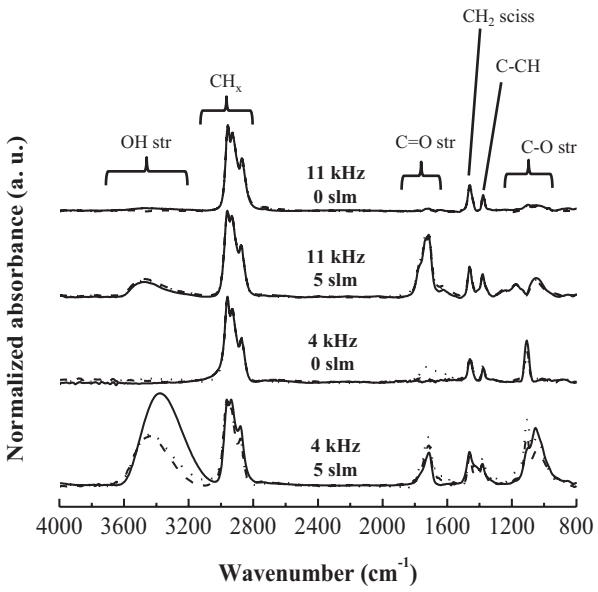

Figure 9. FTIR absorption spectra of coatings before (continuous line) and after water immersion for 1 (dashed line) and 7 d (dot line).

variation. Nearly no difference in the spectra have been found for the coatings that shows no thickness changes (i.e., deposited without water aerosol addition or at high frequency). An intensity decrease in OH stretching band (3 636–3 150 cm^{-1}) can be observed after water immersion for the OH-rich coating. In this case (4 kHz), the calculated area intensities ratio OH/CH clearly reveals a reduction from 2.8 to 1.3 upon 1 d immersion. No further change of intensity ratio was found while passing from 1 to 7 d in water. Nevertheless, it can be affirmed that the relative OH content in this coating, even after the loss during water soaking, remains higher than the value found for the samples obtained at higher power density, which never passes 0.42.

4. Conclusion

Hydroxyl functionalized hydrocarbon films have been successfully deposited using a water aerosol-assisted APP DBD deposition system with ethylene as precursor and helium as buffer gas. Different applied power frequency (4 and 11 kHz) and atomizer flow rate (0–5 slm) were investigated.

The atomization of water combined with ethylene gas feed lead to the rapid deposition of highly functionalized plasma coatings. The results show a high selectivity toward the introduction of —OH groups in the coating, and high deposition rate when the deposition process is run at 4 kHz. At 11 KHz, instead, because of the higher power density,

lower OH selectivity and deposition rate are observed, very likely due to the enhanced fragmentation of the feed and to the higher density of oxygen atoms, which implies etching reactions competing with the deposition process. Films deposited at 11 KHz show a very good stability in water. Coatings deposited at 4 KHz with the highest water aerosol flow rate, in spite of some reduction of OH density during the 1st day of water soaking, show the highest density of OH groups, stable for prolonged immersion in water. Thus, the aerosol-assisted APP deposition has been proved to be feasible for preparing organic coatings bearing hydroxyl groups with potential application in the biomedical field. Such coatings can be used for binding, once rinsed in water, suitable biomolecules, or on the other hand can be a matrix for embedding, using similar aerosol-assisted processing, pharmaceutical agents for drug release devices.

Acknowledgements: The authors show gratitude to the National Science Council (Taiwan) for the grant support 102-2917-I-009-030 to Y.-W. Yang. The projects LIPP (Apulian Industrial Plasma Lab, Rete di Laboratorio Regione Puglia) and RINOVATIS (Regenerating Nervous and Osteocartilagineous Tissues by Means of Innovative Tissue Engineering Approaches, PON, MIUR) are gratefully acknowledged for funding. This research is included in the EC COST action MP1101 "Biomedical Applications of Atmospheric Pressure Plasma Technology." Mr. Savino Cosmai (IMIP-CNR) and Mr. Danilo Benedetti (University of Bari) are acknowledged for their valuable technical assistance.

Received: May 1, 2014; Revised: June 13, 2014; Accepted: June 23, 2014; DOI: 10.1002/ppap.201400066

Keywords: aerosol-assisted deposition; DBD; hydroxyl groups; plasma polymerization

[1] M. Gu, J. E. Kilduff, G. Belfort, *Biomaterials* **2012**, *33*, 1261.
[2] F. Basarir, N. Cuong, W.-K. Song, T.-H. Yoon, *Macromol. Symp.* **2007**, *249–250*, 61.
[3] Y. J. Wu, R. B. Timmons, J. S. Jen, F. E. Molock, *Colloids Surf. B Biointerfaces* **2000**, *18*, 235.
[4] A. M. Sandstrom, M. Jasieniak, H. J. Griesser, L. Grøndahl, J. J. Cooper-White, *Plasma Process. Polym.* **2013**, *10*, 19.
[5] B. Finke, F. Luethen, K. Schroeder, P. D. Mueller, C. Bergemann, M. Frant, A. Ohl, B. J. Nebe, *Biomaterials* **2007**, *28*, 4521.
[6] R. M. France, R. D. Short, E. Duval, F. R. Jones, R. A. Dawson, S. MacNeil, *Chem. Mater.* **1998**, *10*, 1176.
[7] I. Gancarz, J. Bryjak, M. Bryjak, G. Poniak, W. Tylus, *Eur. Polym. J.* **2003**, *39*, 1615.
[8] Y.-W. Yang, J.-Y. Wu, C.-T. Liu, G.-C. Liao, H.-Y. Huang, R.-Q. Hsu, M.-H. Chiang, J.-S. Wu, *J. Biomed. Mater. Res. A* **2013**, *102*, 160.
[9] V. M. Kochkodan, V. K. Sharma, *J. Environ. Sci. Health Part A* **2012**, *47*, 1713.
[10] L. De Bartolo, S. Morelli, A. Piscioneri, L. C. Lopez, P. Favia, R. d'Agostino, E. Drioli, *Biomol. Eng.* **2007**, *24*, 23.
[11] S. Salerno, A. Piscioneri, S. Laera, S. Morelli, P. Favia, A. Bader, E. Drioli, L. De Bartolo, *Biomaterials* **2009**, *30*, 4348.
[12] E. Sardella, L. Detomaso, R. Gristina, G. S. Senesi, H. Agheli, D. S. Sutherland, R. d'Agostino, P. Favia, *Plasma Process. Polym.* **2008**, *5*, 540.
[13] S. Pavlica, A. Piscioneri, F. Peinemann, M. Keller, J. Milosevic, A. Staeudte, A. Heilmann, M. Schulz-Siegmund, S. Laera, P. Favia, L. De Bartolo, A. Bader, *Biomaterials* **2009**, *30*, 6514.
[14] S. Mourtas, M. Kastellorizios, P. Klepetsanis, E. Farsari, E. Amanatides, D. Mataras, B. R. Pistillo, P. Favia, E. Sardella, R. d'Agostino, S. G. Antimisiaris, *Colloids Surf. B Biointerfaces* **2011**, *84*, 214.
[15] F. Intranuovo, E. Sardella, R. Gristina, M. Nardulli, L. White, D. Howard, K. M. Shakesheff, M. R. Alexander, P. Favia, *Surf. Coat. Technol.* **2011**, *205* (Suppl. 2), S548.
[16] B. R. Pistillo, A. Perrotta, R. Gristina, G. Ceccone, M. Nardulli, R. d'Agostino, P. Favia, *Surf. Coat. Technol.* **2011**, *205* (Suppl. 2), S534.
[17] M. Kastellorizios, G. P. A. K. Michanetzis, B. R. Pistillo, S. Mourtas, P. Klepetsanis, P. Favia, E. Sardella, R. d'Agostino, Y. F. Missirlis, S. G. Antimisiaris, *Int. J. Pharm.* **2012**, *432*, 91.
[18] G. Da Ponte, E. Sardella, F. Fanelli, R. d'Agostino, R. Gristina, P. Favia, *Plasma Process. Polym.* **2012**, *9*, 1176.
[19] M. Magliulo, A. Mallardi, M. Y. Mulla, S. Cotrone, B. R. Pistillo, P. Favia, I. Vikholm-Lundin, G. Palazzo, L. Torsi, *Adv. Mater.* **2013**, *25*, 2090.
[20] M. Magliulo, B. R. Pistillo, M. Y. Mulla, S. Cotrone, N. Ditaranto, N. Cioffi, P. Favia, L. Torsi, *Plasma Process. Polym.* **2013**, *10*, 102.
[21] E. Sardella, F. Liuzzi, R. Comparelli, N. Depalo, M. Striccoli, A. Agostiano, P. Favia, M. L. Curri, *Nanotechnology* **2013**, *24*, 145302.
[22] Z. You, H. Cao, J. Gao, P. H. Shin, B. W. Day, Y. Wang, *Biomaterials* **2010**, *31*, 3129.
[23] T. G. Vargo, E. J. Bekos, Y. S. Kim, J. P. Ranieri, R. Bellamkonda, P. Aebischer, D. E. Margevich, P. M. Thompson, F. V. Bright, J. A. Gardella, *J. Biomed. Mater. Res.* **1995**, *29*, 767.
[24] W. W. Gerhardt, D. E. Noga, K. I. Hardcastle, A. J. García, D. M. Collard, M. Weck, *Biomacromolecules* **2006**, *7*, 1735.
[25] M. Leemhuis, C. F. van Nostrum, J. A. W. Kruijtzer, Z. Y. Zhong, M. R. ten Breteler, P. J. Dijkstra, J. Feijen, W. E. Hennink, *Macromolecules* **2006**, *39*, 3500.
[26] Q. Hao, J. Yang, Q. Li, Y. Li, L. Jia, Q. Fang, A. Cao, *Biomacromolecules* **2005**, *6*, 3474.
[27] S. Ponsart, J. Coudane, M. Vert, *Biomacromolecules* **2000**, *1*, 275.
[28] J. Friedrich, *Plasma Process. Polym.* **2011**, *8*, 783.
[29] R. Morent, N. De Geyter, T. Jacobs, S. Van Vlierberghe, P. Dubruel, C. Leys, E. Schacht, *Plasma Process. Polym.* **2009**, *6*, S537.
[30] J.-P. Chen, C.-Y. Kuo, W.-L. Lee, *Appl. Surf. Sci.* **2012**, *262*, 95.
[31] F. Fally, I. Virlet, J. Riga, J. J. Verbist, *J. Appl. Polym. Sci.* **1996**, *59*, 1569.
[32] Y.-M. Ko, K. Lee, B.-H. Kim, *Thin Solid Films* **2012**, *521*, 128.
[33] C. L. Rinsch, X. Chen, V. Panchalingam, R. C. Eberhart, J.-H. Wang, R. B. Timmons, *Langmuir* **1996**, *12*, 2995.
[34] E. R. Leber, B. D. Ratner, *Plasma Process. Polym.* **2009**, *6*, 219.
[35] D. Mangindaan, W.-H. Kuo, C.-C. Chang, S.-L. Wang, H.-C. Liu, M.-J. Wang, *Surf. Coat. Technol.* **2011**, *206*, 1299.
[36] S. Swaraj, U. Oran, A. Lippitz, J. F. Friedrich, W. E. S. Unger, *Surf. Coat. Technol.* **2005**, *200*, 494.
[37] E. Sardella, P. Favia, E. Dilonardo, L. Petrone, R. d'Agostino, *Plasma Process. Polym.* **2007**, *4*, S781.
[38] M. Buttiglione, F. Vitiello, E. Sardella, L. Petrone, M. Nardulli, P. Favia, R. d'Agostino, R. Gristina, *Biomaterials* **2007**, *28*, 2932.

[39] K. S. Siow, L. Britcher, S. Kumar, H. J. Griesser, *Plasma Process. Polym.* **2006**, *3*, 392.
[40] Y.-W. Yang, J.-Y. Wu, M.-H. Chiang, J.-S. Wu, *IEEE Trans. Plasma Sci.* **2012**, *40*, 3003.
[41] M. H. Chiang, J. Y. Wu, Y. H. Li, J. S. Wu, S. H. Chen, C. L. Chang, *Surf. Coat. Technol.* **2010**, *204*, 3729.
[42] G. Da Ponte, E. Sardella, F. Fanelli, R. d'Agostino, P. Favia, *Eur. Phys. J. – Appl. Phys.* **2011**, *56*, 24023.
[43] M.-H. Chiang, K.-C. Liao, I.-M. Lin, C.-C. Lu, H.-Y. Huang, C.-L. Kuo, J.-S. Wu, *IEEE Trans. Plasma Sci.* **2010**, *38*, 1489.
[44] M.-H. Chiang, K.-C. Liao, I.-M. Lin, C.-C. Lu, H.-Y. Huang, C.-L. Kuo, J.-S. Wu, C.-C. Hsu, S.-H. Chen, *Plasma Chem. Plasma Process.* **2010**, *30*, 553.
[45] I. Topala, N. Dumitrascu, G. Popa, *Nucl. Instrum. Methods Phys. Res. Sect. B Beam Interact. Mater. Atoms* **2009**, *267*, 442.
[46] D. Kurniawan, B. S. Kim, H. Y. Lee, J. Y. Lim, *Compos. Part B Eng.* **2012**, *43*, 1010.
[47] O. Carton, D. Ben Salem, S. Bhatt, J. Pulpytel, F. Arefi-Khonsari, *Plasma Process. Polym.* **2012**, *9*, 984.
[48] A. J. Beck, R. D. Short, A. Matthews, *Surf. Coat. Technol.* **2008**, *203*, 822.
[49] T. P. Kasih, S. Kuroda, H. Kubota, *Plasma Process. Polym.* **2007**, *4*, 648.
[50] G. Da Ponte, E. Sardella, F. Fanelli, S. Paulussen, P. Favia, *Plasma Process. Polym.* **2014**, *11*, 345.
[51] U. Oran, S. Swaraj, J. F. Friedrich, W. E. S. Unger, *Plasma Process. Polym.* **2005**, *2*, 563.
[52] S. Swaraj, U. Oran, A. Lippitz, J. F. Friedrich, W. E. S. Unger, *Plasma Process. Polym.* **2005**, *2*, 572.
[53] B. M. Wickson, J. L. Brash, *Colloids Surf. Physicochem. Eng. Asp.* **1999**, *156*, 201.
[54] G. S. Malkov, E. R. Fisher, *Plasma Process. Polym.* **2010**, *7*, 695.
[55] A. Fahmy, R. Mix, A. Schönhals, J. F. Friedrich, *Plasma Chem. Plasma Process.* **2011**, *31*, 477.
[56] V. Ley, A. P. Kruzic, R. B. Timmons, *J. Membr. Sci.* **2003**, *226*, 213.
[57] S. Swaraj, U. Oran, J. F. Friedrich, A. Lippitz, W. E. S. Unger, *Plasma Process. Polym.* **2007**, *4*, 376.
[58] S. Farhat, M. Gilliam, M. Rabago-Smith, C. Baran, N. Walter, A. Zand, *Surf. Coat. Technol.* **2014**, *241*, 123.
[59] R. Thyen, A. Weber, C.-P. Klages, *Surf. Coat. Technol.* **1997**, *97*, 426.
[60] J. Bardon, J. Bour, H. Aubriet, D. Ruch, B. Verheyde, R. Dams, S. Paulussen, R. Rego, D. Vangeneugden, *Plasma Process. Polym.* **2007**, *4*, S445.
[61] L.-A. O'Hare, L. O'Neill, A. J. Goodwin, *Surf. Interface Anal.* **2006**, *38*, 1519.
[62] P. Heyse, A. Van Hoeck, M. B. J. Roeffaers, J.-P. Raffin, A. Steinbüchel, T. Stöveken, J. Lammertyn, P. Verboven, P. A. Jacobs, J. Hofkens, S. Paulussen, B. F. Sels, *Plasma Process. Polym.* **2011**, *8*, 965.
[63] P. Heyse, R. Dams, S. Paulussen, K. Houthoofd, K. Janssen, P. A. Jacobs, B. F. Sels, *Plasma Process. Polym.* **2007**, *4*, 145.
[64] P. Heyse, M. B. J. Roeffaers, S. Paulussen, J. Hofkens, P. A. Jacobs, B. F. Sels, *Plasma Process. Polym.* **2008**, *5*, 186.
[65] L. J. Ward, W. C. E. Schofield, J. P. S. Badyal, A. J. Goodwin, P. J. Merlin, *Chem. Mater.* **2003**, *15*, 1466.
[66] T. J. Wood, P. S. Brown, J. P. S. Badyal, *Chem. Commun.* **2013**, *49*, 7741.
[67] T. J. Wood, J. P. S. Badyal, *Surf. Coat. Technol.* **2013**, *227*, 28.
[68] F. Fanelli, F. Fracassi, R. d'Agostino, *Plasma Process. Polym.* **2005**, *2*, 688.
[69] O. Goossens, E. Dekempeneer, D. Vangeneugden, R. Van de Leest, C. Leys, *Surf. Coat. Technol.* **2001**, *142–144*, 474.
[70] L. M. Martini, G. Dilecce, M. Scotoni, P. Tosi, S. D. Benedictis, *Plasma Process. Polym.* **2014**, *11*, 232.
[71] A. Fahmy, R. Mix, A. Schönhals, J. Friedrich, *Plasma Chem. Plasma Process.* **2012**, *32*, 767.
[72] P. Bruggeman, F. Iza, P. Guns, D. Lauwers, M. G. Kong, Y. A. Gonzalvo, C. Leys, D. C. Schram, *Plasma Sources Sci. Technol.* **2010**, *19*, 015016.
[73] G. Dilecce, S. D. Benedictis, *Plasma Phys. Control. Fusion* **2011**, *53*, 124006.
[74] M. L. Steen, C. I. Butoi, E. R. Fisher, *Langmuir* **2001**, *17*, 8156.
[75] J. Peeters, S. Vandenberk, E. Piessens, V. Pultau, *Chemosphere* **1999**, *38*, 1189.
[76] A. N. Bhoj, M. J. Kushner, *J. Phys. D: Appl. Phys.* **2007**, *40*, 6953.